Article

A Strand-Loop-Strand Structure Is a Possible Intermediate in Fibril Elongation: Long Time Simulations of Amyloid-β Peptide (10–35)

Wei Han, and Yun-Dong Wu

J. Am. Chem. Soc., **2005**, 127 (44), 15408-15416• DOI: 10.1021/ja051699h • Publication Date (Web): 13 October 2005

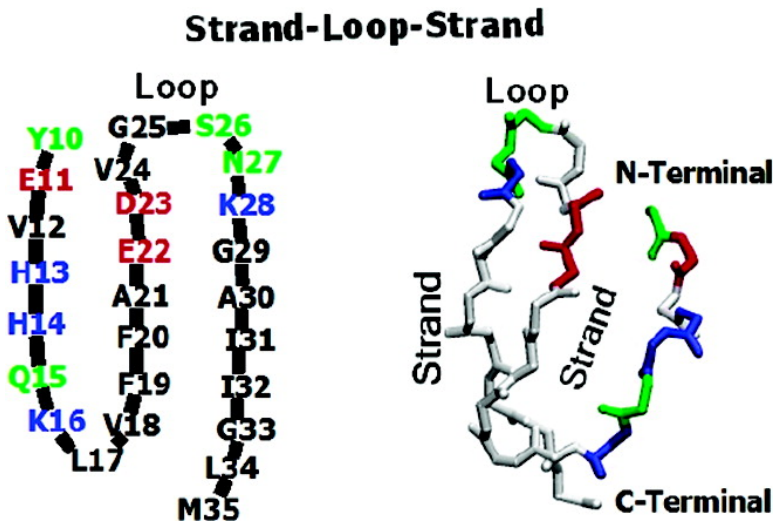

More About This Article

Additional resources and features associated with this article are available within the HTML version:

- Supporting Information
- Links to the 13 articles that cite this article, as of the time of this article download
- Access to high resolution figures
- Links to articles and content related to this article
- Copyright permission to reproduce figures and/or text from this article

View the Full Text HTML

J|A|C|S
ARTICLES
Published on Web 10/13/2005

A Strand-Loop-Strand Structure Is a Possible Intermediate in Fibril Elongation: Long Time Simulations of Amyloid-β Peptide (10−35)

Wei Han[†] and Yun-Dong Wu*[,†,‡]

Contribution from the Department of Chemistry, The Hong Kong University of Science & Technology, Clear Water Bay, Kowloon, Hong Kong, China, and State Key Lab of Molecular Dynamics and Stable Structures, College of Chemistry, Peking University, Beijing, China

Received March 17, 2005; E-mail: chydwu@ust.hk

Abstract: A total of 6.2 μs molecular dynamics simulations of amyloid-β (10−35) (Aβ) were performed in explicit water solvent. The results reveal that the collapsed-coil (cc) structure determined by experiments is stable at pH 5.6 for hundreds of nanoseconds, but it can exchange with a strand-loop-strand (SLS) structure on the microsecond time scale. The SLS structure has D23−K28 as a reverse loop and the central hydrophobic core and the C-terminal in hydrophobic contact. This SLS structure topologically resembles the proposed monomer conformation in fibrils. Since it has been suggested that a special conformation of Aβ is needed when the monomer binds to fibril ends to elongate fibrils, we propose that the SLS structure may be an important intermediate binding structure for Aβ fibril growth. Simulations at pH 2.0, which is used to mimic the mutation of E22Q and D23N, and at high temperature (400 K) indicate that the SLS structure is considerably populated under these conditions while the cc structure is disrupted. These results imply that the SLS structures may also be a binding intermediate in other conditions such as E22Q and/or D23N mutations and high temperature, which have been proved to promote fibril formation previously.

Introduction

Cerebral amyloid plaques, composed of fibrillar forms of amyloid-β peptide (Aβ) with 39−43 amino acid residues,[1] are the hallmark of Alzheimer's disease (AD).[2] The aggregation of Aβ fibrils has been suspected to be an early and required event in AD and to be related to its etiology, known as the amyloid hypothesis.[3−6] This notion is supported by in vitro cell culture experiments, the correlation between the density of deposits and progressive neurodegeneration, and genetic studies that show mutations in early-onset familial AD can increase the production of Aβ42, accelerating amyloid formation. Since the inhibition of amyloid formation may benefit AD therapies,[7] it is important to understand the mechanism of the Aβ conformational transition and assembly from the monomer in solution to the β-sheet-rich amyloid.[8]

In fibrils, Aβ is known to adopt a parallel β-sheet conformation.[9] Tycko et al. discovered by solid-state NMR that the V25−G29 region adopts a non-β conformation (Figure 1a).[10] They suggested that this region can form a bend and bring the two β-sheets, V12−V24 and A30−V40, into contact.[10,11] This suggestion was supported by other experiments and by the molecular modeling.[12−14] On the basis of solution NMR results, Lee and Zhang et al. proposed that Aβ(10−35) adopts a collapsed-coil (cc) structure in water at pH 5.6 (Figure 1b).[15,16] Such a structure has an ordered core (L17−K28) and flexible C- and N-terminals. The core and the C-terminal consist of several sequential sharp turns and bind together through hydrophobic interactions. The N-terminal folds back onto the core through hydrophobic and electrostatic interactions. The molecule is amphiphilic in nature with a large exposed hydrophobic surface.

In vitro studies have suggested that Aβ fibrillogenesis includes nucleation and fiber elongation.[17] After nucleation, Aβ monomers in solution can be directly incorporated into the nuclei to

[†] The Hong Kong University of Science & Technology.
[‡] Peking University.

(1) Sisodia, S. S.; Koo, E. H.; Beyreuther, K.; Unterbeck, A.; Price, D. L. *Science* **1990**, *248*, 492−495.
(2) Lansbury, P. T., Jr. *Acc. Chem. Res.* **1996**, *29*, 317−321.
(3) Selkoe, D. *Science* **1997**, *275*, 630−631.
(4) Yankner, B. A.; Duffy, L. K.; Kirschner, D. A. *Science* **1990**, *250*, 279−282.
(5) Selkoe, D. *J. Neuropathol. Exp. Neurol.* **1994**, *53*, 438−447.
(6) Jarrett, J. T.; Berger, E. P.; Lansbury, P. T., Jr. *Biochemistry* **1993**, *32*, 4693−4697.
(7) Mason, J. M.; Kokkoni, N.; Stott, K.; Doig, A. J. *Curr. Opin. Struct. Biol.* **2003**, *13*, 526−532.
(8) Lansbury, P. T., Jr. *Curr. Opin. Chem. Biol.* **1997**, *1*, 260−267.
(9) Benzinger, T. L. S.; Gregory, D. M.; Burkoth, T. S.; Miller-Auer, H.; Lynn, D. G.; Botto, R. E.; Meredith, S. C. *Proc. Natl. Acad. Sci. U.S.A.* **1998**, *95*, 13407−13412.
(10) Antzutkin, O. N.; BalBach, J. J.; Tycko, R. *Biophys. J.* **2003**, *84*, 3326−3335.
(11) Petkova, A. T.; Ishii, Y.; Balbach, J. J.; Antzutkin, O. N.; Leapman, R. D.; Delaglio, F.; Tycko, R. *Proc. Natl. Acad. Sci. U.S.A.* **2002**, *99*, 16742−16747.
(12) Torok, M.; Milton, S.; Kayed, R.; Wu, P.; McIntire, T.; Glabe, C. G.; Langen, R. *J. Biol. Chem.* **2002**, *277*, 40810−40815.
(13) Shivaprasad, S.; Wetzel, R. *Biochemistry* **2004**, *43*, 15310−15317.
(14) Ma, B.; Nossinov, R. *Proc. Natl. Acad. Sci.* **2002**, *99*, 14126.
(15) Lee, J. P.; Stimson, E. R.; Ghilardi, J. R.; Mantyh, P. W.; Lu, Y. A.; Felix, A. M.; Lianos, W.; Behbin, A.; Cummings, M.; Criekinges, M. V.; et al. *Biochemistry* **1995**, *34*, 5191−5200.
(16) Zhang, S.; Iwata, K.; Lachenmann, M. J.; Peng, J. W.; Li, S.; Stimson, E. R.; Lu, Y. A.; Felix, A. M.; Maggio, J. E.; Lee, J. P. *J. Struct. Biol.* **2000**, *130*, 130−141.

10.1021/ja051699h CCC: $30.25

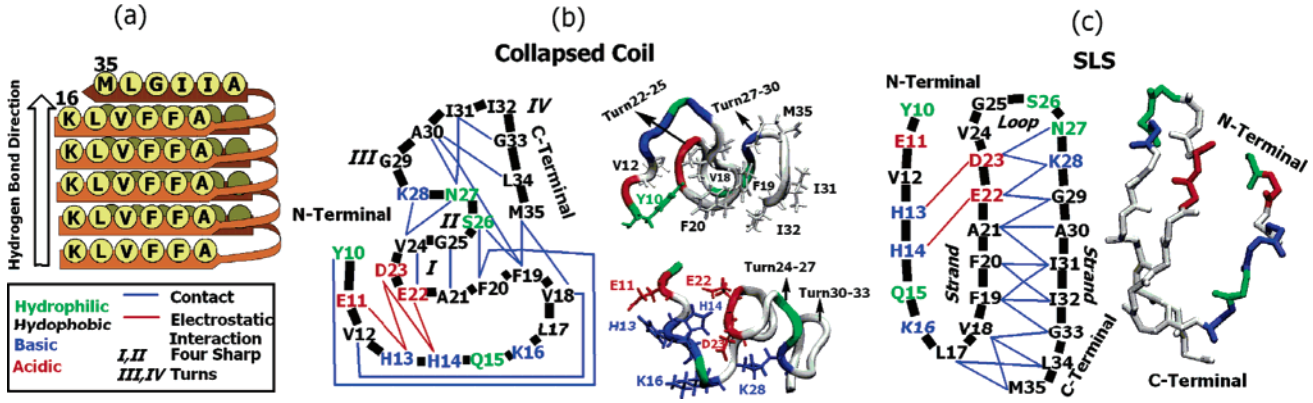

Figure 1. (a) Proposed double-layered bend structure in the fibril. (b) Collapsed-coil structure derived by the experiment (right) and its schematic representation (left). (c) Strand-loop-strand structure found in our study (left) and its schematic representation (right).

elongate the fibrils.[18−20] Consequently, the difference between the Aβ conformation in solution and that in fibrils implies that Aβ is involved in a large conformational change during the fibril growth, while Aβ monomer conformation in solution may influence this process.[15] It was found that Aβ(1−28) and Aβ-(10−35)/(1−40) at pH 2.0 or with the F19T mutation did not deposit onto the authentic plaque of AD patients.[21] Since they are less folded than Aβ(10−35)/(1−40) at pH 5.6, which has a cc structure, this finding and the following kinetics study have led to a suggestion that this cc structure might be required for docking the Aβ monomer onto the fibril end during elongation and thus be a potential target for amyloid inhibition.[22]

Two aggregation-promoting mutations, E22Q and D23N, have been found in early-onset familial AD, named as Dutch and Iowa types, respectively.[23,24] Either of them in Aβ(1−40) can accelerate fibril formation, and double mutations can further enhance aggregation.[25,26] The change caused by the mutations is substitution of charged carboxylic groups with neutral amide groups. This is quite similar to the situation at low pH, where E22 and D23 are protonated. However, Aβ(10−35)/(1−40) cannot adopt the cc structure under this condition. Thus it raises the question of whether there is any monomeric conformation other than the cc structure that may be related to the fibril growth of the mutations. Another question is if a special conformation is required for the docking step during the fiber formation,[16,22] it should be at least marginally stable at high temperature since high temperature promotes aggregation or fibril elongation at varying pH.[25,27,28] Such enhancement persists even up to 371 K.[29] These questions lead us to study the stability and dynamics of Aβ monomer conformation under different conditions, such as varying temperature and pH.

Aβ monomer and its fragments have been the subject of many molecular dynamics (MD) simulations in explicit water to give useful atomistic information. The first study of the cc structure was done by Straub and co-workers.[30−32] They performed multiple simulations to systematically examine the stability and dynamics of Aβ(10−35) and its mutants shortly after this structure was derived from experiments. Valerio et al. studied Aβ(1−40) at distinct pHs by multiple simulations in water and suggested that the flexibility of Aβ correlates with aggregation propensities, based on the membrane-mimicking conformation.[33] Those studies focused on local conformations of Aβ. Recently, Daidone et al. observed a large conformational change and the appearance of a hairpin-like structure of Aβ(12−28) during their 100 ns simulation in water.[34] In this paper, we report on molecular dynamics simulations of Aβ(10−35) up to 1.2 μs at pH 5.6 to test the dynamics of Aβ. Simulations were also carried out at pH 2 (1.3 μs) to mimic the double mutations of E22Q and D23N and at high temperature (400 K, totally 2.0 μs) to test the thermostability of Aβ. The results indicate that a strand-loop-strand (SLS) structure (Figure 1c), which has a topology similar to that of Aβ monomer in fibrils, may be an important intermediate structure responsible for fibril elongation.

Methods

MD Simulations. All MD simulations were performed with the GROMACS software package.[35,36] The starting conformation came from Protein Data Bank, entry code 1HZ3.[16] Single-point charge (SPC) water was used in all simulations.[37,38] The SETTLE algorithm was used to

(17) Jarrett, J. T.; Lansbury, P. T., Jr. *Cell* **1993**, *73*, 1055−1058.
(18) Lomakin, A.; Chung, D. S.; Benedek, G. B.; Kirschner, D. A.; Teplow, D. B. *Proc. Natl. Acad. Sci. U.S.A.* **1996**, *93*, 1125−1129.
(19) Naiki, H.; Nakakuki, K. *Lab. Invest.* **1996**, *74*, 374−383.
(20) Esler, W. P.; Stimson, E. R.; Ghilardi, J. R.; Vinters, H. V.; Lee, J. P.; Mantyh, P. W.; Maggio, J. E. *Biochemistry* **1996**, *35*, 749−757.
(21) Esler, W. P.; Stimson, E. R.; Ghilardi, J. R.; Lu, Y. A.; Felix, A. M.; Vinters, H. V.; Mantyh, P. W.; Lee, J. P.; Maggio, J. E. *Biochemistry* **1996**, *35*, 13914−13921.
(22) Esler, W. P.; Stimson, E. R.; Jennings, J. M.; Vinters, H. V.; Ghilardi, J. R.; Lee, J. P.; Mantyh, P. W.; Maggio, J. E. *Biochemistry* **2000**, *39*, 6288−6295.
(23) Levy, E.; Carman, M. D.; Fernandezmadrid, I. J.; Power, M. D.; Lieberburg, I.; Vanduinen, S. G.; Bots, G. T. A. M.; Luyendijk, W.; Fragione, B. *Science* **1990**, *248*, 1124−1126.
(24) Grabowski, T. J.; Cho, H. S.; Vonsattel, J. P. G.; Rebeck, G. W.; Greenberg, S. M. *Ann. Neurol.* **2001**, *49*, 697−705.
(25) Esler, W. P.; Felix, A. M.; Stimson, E. R.; Lachenmann, M. J.; Ghilardi, J. R.; Lu, Y. A.; Vinters, H. V.; Mantyh, P. W.; Lee, J. P.; Maggio, J. E. *J. Struct. Biol.* **2000**, *130*, 174−183.
(26) van Nostrand, W. E.; Melchor, J. P.; Cho, H. S.; Greenberg, S. M.; Rebeck, G. W. *J. Biol. Chem.* **2001**, *276*, 32860−32866.
(27) Kusumoto, Y.; Lomakin, A.; Teplow, D. B.; Benedek, G. B. *Proc. Natl. Acad. Sci. U.S.A.* **1998**, *95*, 12277−12282.
(28) Snyder, S. W.; Ladror, U. S.; Wade, W. S.; Wang, G. T.; Barrett, L. W.; Matayoshi, E. D.; Huffaker, H. J.; Krafft, G. A.; Holzman, T. F. *Biophys. J.* **1994**, *67*, 1216−1228.
(29) Gursky, O.; Aleshkov, S. *Biochim. Biophys. Acta* **2000**, *1476*, 93−102.
(30) Massi, F.; Peng, J. W.; Lee, J. P.; Straub, J. E. *Biophys. J.* **2001**, *80*, 31−44.
(31) Massi, F.; Straub, J. E. *Biophys. J.* **2001**, *81*, 697−709.
(32) Massi, F.; Klimov, D.; Thirumalai, D.; Straub, J. E. *Protein Sci.* **2002**, *11*, 1639−1647.
(33) Valerio, M.; Colosimo, A.; Conti, F.; Giuliani, A.; Grottesi, A.; Manetti, C.; Zbilut, J. P. *Proteins* **2005**, *58*, 110−118.
(34) Daidone, I.; Simona, F.; Roccatano, D.; Broglia, R. A.; Tiana, G.; Colombo, G.; Nola, A. D. *Proteins* **2004**, *57*, 198−204.
(35) Berendsen, H. J. C.; van der Spoel, D.; van Drunen, R. *Comput. Phys. Commun.* **1995**, *91*, 43−56.
(36) Van der Spoel, D.; van Buuren, A. R.; Apol, E.; Meulenhoff, P. J.; Tieleman, D. P.; Sijbers, A. L. T. M.; Hess, B.; Feenstra, K. A.; Lindahl, E.; van Drunen, R.; Berendsen, H. J. C. *GROMACS user manual, version 3.1*; Groningen, 2002.

Table 1. Setup Details of the Three Simulations and Their Clustering Results

name	starting[a] conformation	T (K)	pH[b]	nonbonded cutoff (nm)	total time (μs)	number of frames	number of clusters	number of transitions[d]
AβHpH	1st	300	5.6	1.0	1.2	120 000	55	164
AβLpH	1st	300	2	1.0	1.3	130 000	143	347
AβHT	1st, 9th	400	5.6	0.9/1.4[c]	2.0	1 000 000	2308	18 970

[a] The first and ninth models of 1HZ3 were used as the starting conformation for most of the simulations. In AβHT, each of them was used for 10 simulations with different initial velocities. [b] All Lys and His are protonated. At pH 2.0, Asp and Glu are neutral, while they are charged at pH 5.6. [c] Twin-range cutoff. [d] If cluster i can transit to cluster j, such a transition is one type.

constrain the bond length and angle of the water.[39] The bond lengths of the peptide were constrained by the LINCS algorithm.[40] All simulations were under constant temperature and pressure coupled with an external thermostat and a pressure bath with coupling constants of 0.1 and 1.0 ps, respectively.[41] Before each production run, the system was subjected to a 2000-step steep descent optimization, followed by a 200 ps MD equilibrium simulation with position restraints on the peptide atoms. GROMACS, GROMOS96 43A1, and OPLS-AA force fields were used in the simulations.[42−44] Particle-mesh Ewald (PME) was used in supporting simulations to examine the cutoff effect on long-range electrostatic interactions and the stabilities of the cc structure and the SLS structure at various conditions (listed in Table S1).[45] Table 1 lists some simulation setups, while more detailed setup information is given in the Supporting Information.

Contact Map. A pair of residues, i and j ($j > i + 2$), are regarded as in contact if the distance between two closest heavy atoms of the two residues is less than 0.54 nm.[46] Thus, the contacts of all pairs of residues of a conformation can be represented by a 2-D matrix $H(i,j)$. $H(i,j)$ equals 1 if residues i and j are in contact and equals zero otherwise. A contact map is a 3-D graph to visualize the contact pattern of a conformation ensemble using the contact frequency, $G(i,j)$, between each pair of residues over the whole conformation ensemble.

Contact Score. The similarity and dissimilarity of a conformation H with respect to a conformation ensemble G can be reflected by a contact score C. Here, C is calculated on the basis of eq 1.

$$C = \sum_{i<j} \sigma_{ij}, \sigma_{ij} = \begin{cases} 1.5 & \text{if } H(i,j) = 1 \,\&\, G(i,j) > 0.75; \\ 1.0 & \text{if } H(i,j) = 1 \,\&\, 0.75 \geq G(i,j) > 0.50; \\ -0.5 & \text{if } H(i,j) = 1 \,\&\, G(i,j) < 0.25; \\ 0.0 & \text{otherwise} \end{cases} \quad (1)$$

This is analogous to the common contact number, defined as the contact matrix overlap of two conformations, which reflects the similarity of tertiary contact patterns and raw topologies between the two conformations.[46,47] Our C score is distinct because (1) it compares a conformation with an ensemble and (2) it also enumerates the dissimilarity of the conformation with the ensemble.

Cluster Analysis. All the collected conformations are clustered as described by Daura et al.[48] After superimposition, the root-mean-square deviation (RMSD) of any two given conformations is calculated according to all C_α's. The cutoff for neighbor counting is set to 0.25 nm. When any two sequential frames belong to two different clusters, the transition between these two clusters is counted. The results for the three simulations are shown in Table 1.

Transition Disconnectivity Graph. The transition disconnectivity graph (TRDG) is a pictorial representation of the free energy (FE) surface of a peptide.[49] An equilibrium trajectory can provide the FE of states (the times the system visited this state) and barriers between them (the times the system transits from state i to j). TRDG is a tree-like graph, where nodes indicate the FE minima and branch points indicate transition barriers. It can partition states on the basis of their barriers. The states with low barriers are clustered into the same basin, while high barriers separate different basins (a simple illustration of the TRDG can be found in the Supporting Information).[50] We constructed the FE surface TRDG from our high-temperature simulation (AβHT) clustering results according to the method described by Karplus et al.[51−53] All the analyses were done with the GROMACS package tools as well as our own codes.

Results and Discussion

Stability and Dynamics of Aβ(10−35) at pH 5.6. The 1.2 μs simulation of Aβ(10−35) at pH 5.6 (AβHpH) can be divided into three stages.

The first stage is 0−200 ns in the simulation. Figure 2a shows the average contact map of the experimentally determined cc structure from 15 models in 1HZ3. A comparison between Figure 2a and Figure 2b, which is the contact map of the conformation ensemble of this stage, indicates that most structural features of the cc structure are conserved. These include sequential sharp β-turns, spanning V24−N27, N27−A30, and A30−G33. In addition, another reverse loop (F19−S26) centered at E22−V24 also persists. F19 and E22/D23 dominate the interaction of the central region (L17−K28) with the C- and N-terminals, respectively. The average contact score C with respect to the cc structure is 25, about half of the maximum value, 70 (Figure 3, black).

The second stage is the period of 200−600 ns. The contact score C with respect to the cc structure is about 10 (Figure 3, black). It can be seen from the contact map of this time period that the loss of similarity with the cc structure is mainly due to the C-terminal (SI, Figure S2a). This is also confirmed by the backbone RMSD calculations, which show that the N-terminal is more like that in the collapsed coil (SI, Figure S3).

The final stage is the period of 600−1200 ns. The C value rapidly drops and stays at about 0 during this period (Figure 3, black). The contact map of this stage (Figure 2c) indicates that

(37) Smith, P. E.; van Gunsteren, W. F. *J. Chem. Phys.* **1994**, *100*, 3169−3174.
(38) van der Spoel, D.; van Maaren, P. J.; Berendsen, H. J. C. *J. Chem. Phys.* **1998**, *108*, 10220−10230.
(39) Miyamoto, S.; Kollman, P. A. *J. Comput. Chem.* **1992**, *13*, 952−962.
(40) Hess, B.; Bekker, H.; Berendsen, H. J. C.; Fraaije, J. G. E. M. *J. Comput. Chem.* **1997**, *18*, 1463−1472.
(41) Beredsen, H. J. C.; Postma, J. P. M.; van Gunsteren, W. F.; Di Nola, A.; Haak, J. R. *J. Chem. Phys.* **1984**, *81*, 3684−3690.
(42) Mark, A. E.; Helden, S. P.; Smith, P. E.; Janssen, L. H. M.; van Gunsteren, G. W. *J. Am. Chem. Soc.* **1994**, *116*, 6293−6302.
(43) van Gunsteren, W. F.; Billeter, S. R.; Eising, A. A.; Hunenberger, P. H.; Kruger, P.; Mark, A. E.; Scott, W. R. P. *Biomolecular simulation: the GROMOS96 manual and user guide*; Hchschulverlag AG an der ETH: Zurich, 1996.
(44) Jorgensen, W. L.; Maxwell, D. S.; Tirado-Rives, J. *J. Am. Chem. Soc.* **1996**, *118*, 11225−11236.
(45) Darden, T.; York, D.; Pedersen, L. *J. Chem. Phys.* **1993**, *98*, 10089−10092.
(46) Kazmirski, S. L.; Li, A. J.; Daggett, V. *J. Mol. Biol.* **1999**, *290*, 283−304.
(47) Sali, A.; Shakhnovich, E.; Karplus, M. *Nature* **1994**, *369*, 248−251.
(48) Daura, X.; Gademann, K.; Jaun, B.; Seebach, D.; van Gunsteren, W. F.; Mark, A. E. *Angew. Chem., Int. Ed.* **1999**, *38*, 236−240.
(49) Krivov, S. V.; Karplus, M. *J. Chem. Phys.* **2002**, *117*, 10894−10903.
(50) Wales, D. J. *Energy Landscapes*; Cambridge University Press: Cambridge, U.K., 2003.
(51) Krivov, S. V.; Karplus, M. *Proc. Natl. Acad. Sci. U.S.A.* **2004**, *101*, 14766−14770.
(52) Ford, L. R.; Fulkerson, D. R. *Can. J. Math.* **1956**, *8*, 399−404.
(53) Gomory, R. E.; Hu, T. C. *SIAM J. Appl. Math.* **1961**, *9*, 551−570.

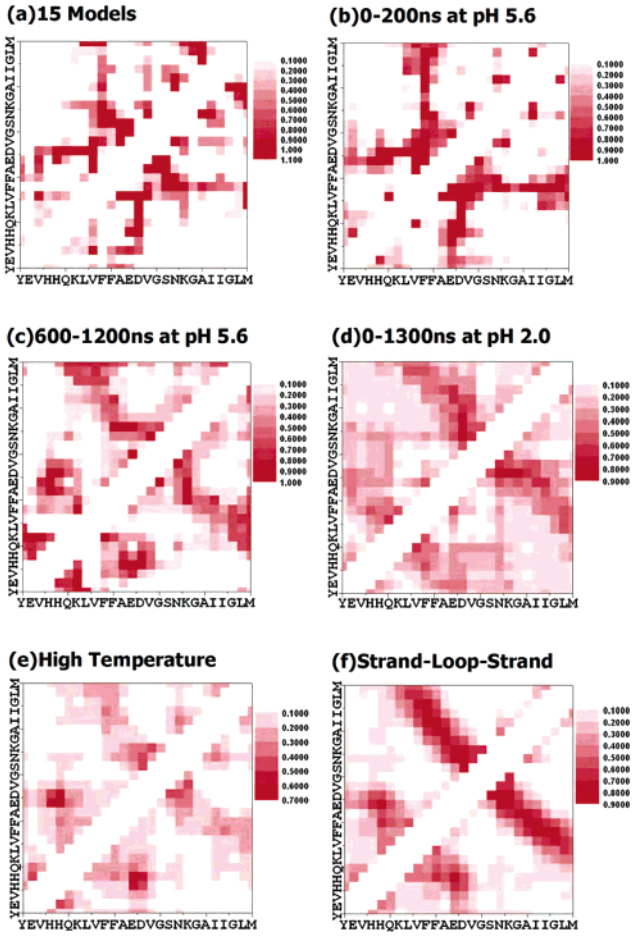

Figure 2. Average contact maps of (a) 15 models from experiments; (b) 0−200 ns simulation of Aβ HpH; (c) 600−1200 ns simulation of Aβ HpH; (d) Aβ LpH simulation; (e) Aβ HT simulations; (f) all SLS-like conformations in the Aβ HT simulations.

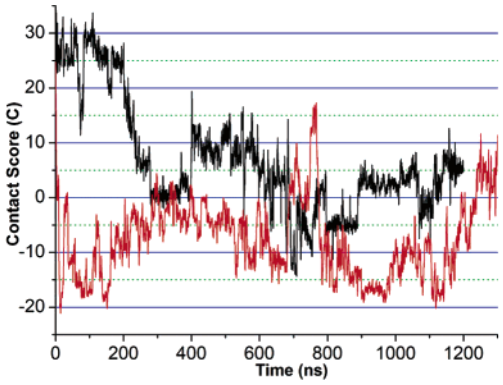

Figure 3. Contact score *C* with respect to the collapsed-coil structure in Aβ HpH (black) and Aβ LpH (red) simulations.

many structural features vanish, most obviously the reverse loop (F19−S26). Instead, another loop centered at V24−S26 is intensified while the C-terminal (A30−M35) contacts more widely with the central hydrophobic core (CHC). The results clearly reveal that a large conformational change occurs in this stage and the molecule enters another conformational region.

The above results reveal that the cc structure derived from the NOE data is dominant in the first 200 ns and partially preserved in the first 600 ns. However, it can exchange with other very distinct conformations within microseconds. This raises the question of whether the cc structure can coexist with other structures. The pioneering work of Mieke et al. showed the importance of ensemble average for NMR structure refinement.[54] Recently, several reports suggested that the 2-D NMR NOE data and ^3J coupling constants that are used to derive a single conformation for a short peptide actually can also be fitted with a set of equilibrium conformations.[55−57] Accordingly, the NOE restraints were recalculated for both experimental structures and our simulations.

Assuming that each model from 1HZ3 (PDB) equally occurs, each NOE distance was calculated by $\langle d^{-6}\rangle^{-1/6}$ as an ensemble average, where d is the inter-hydrogen distance. Only those distances larger than the corresponding NOE upper bounds by 0.05 nm are considered to be NOE violations, as described by Monticelli et al.[58] Among the 547 NOE restraints from experiments,[16] there are 73 violations for the 15 models of 1HZ3, while there are 79 for the whole Aβ HpH trajectory, indicating that the agreement of the simulation with the NOE data is comparable to that of model 1HZ3 structures. The conformational change may not conflict with experimental observations. Actually, an ^{15}N relaxation measurement implied that the conformation exchange of Aβ(10−35) does exist.[30] Another interesting study of the Aβ(10−35) dimer also demonstrated that upon dimerization, Aβ rapidly undergoes a large conformational change from the cc structure.[59] All these support that the cc is metastable and ready to exchange with other structures within the time scale of the NMR measurement.

Stability and Dynamics of Aβ(10−35) at pH 2.0. At pH 2, the cc structure becomes unstable in the Aβ LpH simulation. The contact score *C* with respect to the cc structure rapidly drops down to about −20 in the first few nanoseconds. After that, it rarely goes back above zero even to 1.3 μs (Figure 3, red). The contact map (Figure 2d) indicates that it results from the loss of the loop centered at E22−V24 and the interaction between D23 and the N-terminal (Figure 1b) and from the enhancement of the loop centered at V24−S26 (Figure 1c). A previous NMR experiment indicated that as the pH is raised from 2.1 to 5.6, more contacts between the aromatic side chain of F19 (and/or F20) and the side chains of I31−M35 were observed.[16] Thus we analyzed the total number of contacts between the side chain heavy atoms of these two parts for both Aβ HpH and Aβ LpH simulations. The average numbers of contacts are 36 for Aβ HpH and 19 for Aβ LpH, implying that the F19/20 do have more interactions with the C-terminal at pH 5.6, in agreement with the experimental results.[16]

The only difference between different pH conditions is the charge states of E11, E22, and D23. At low pH, carboxyl anions have to be neutralized. Previous simulations have suggested that the neutralization of the anion groups influences the hydration of the cc structure based on nanosecond trajectories.[31,32] When neutralized, reduced hydration will lower the dissolvation barrier of the peptide and, therefore, promote deposition. Our microsecond time scale simulations allow investigation of its more profound effects on the dynamics and stability of the peptide. The negatively charged Glu and Asp are important for the

(54) Mierke, D. F.; Kurz, M.; Kessler, H. *J. Am. Chem. Soc.* **1994**, *116*, 1042.
(55) Glattli, A.; van Gunsteren, W. F. *Angew. Chem., Int. Ed.* **2004**, *43*, 6312−6316.
(56) Carstens, H.; Renner, C.; Milbradt, A. G.; Moroder, L.; Tavan, P. *Biochemistry* **2005**, published online.
(57) Soto, P.; Colombo, G. *Proteins* **2004**, *57*, 734−746.
(58) Monticelli, L.; Colombo, G. *Theor. Chem. Acc.* **2004**, *112*, 145.
(59) Tarus, B.; Straub, J. E.; Thirumalai, D. *J. Mol. Biol.* **2005**, *345*, 1141.

Table 2. Probabilities of Minimum Distances between Basic and Acidic Groups Shorter than 0.5 nm[a]

	pH 5.6	pH 2.0	400 K
E11−H13	63.4	22.4	36.0
E11−H14	32.4	13.9	25.6
E11−K16	0.6	3.9	1.1
E11−K28	1.8	8.6	0.5
E22−H13	32.3	8.2	31.8
E22−H14	7.9	8.3	58.4
E22−K16	21.1	2.2	4.4
E22−K28	17.9	4.9	4.8
D23−H13	10.5	10.0	43.4
D23−H14	76.9	1.0	36.7
D23−K16	1.9	1.3	3.4
D23−K28	3.3	5.0	5.2

[a] The distance between His and Glu/Asp is the minimum distance between the ϵ/δ-N of His and carboxylic O of Glu/Asp. The distance between Lys and Glu/Asp is the minimum distance between ammonium N of Lys and carboxylic O of Glu/Asp.

stability of the cc structure, since it can exist for about 200 ns at pH 5.6 while is essentially unstable at low pH. As shown in Table 2, at pH 5.6, the salt bridges between H13/H14 and E22/D23 can last for up to 70% of the simulation time. However, at pH 2.0, the salt bridges essentially disappear. This supports the proposal that the carboxyl anions can form salt bridges with the His residues and stabilize the cc structure at pH 5.6.[15]

Additionally, solid-state NMR experiments have shown that D23 and K28 can form a salt bridge in fibrils and stabilize amyloid.[11] To assess the importance of such salt bridge or electrostatic interaction to the stability of Aβ monomer, we analyzed the distance profiles related to K28. According to Figure S4, both E22−K28 and D23−K28 contact distances are broadly distributed in the range of 0.5−1.0 nm. For a normal salt bridge, a sharp contact distance at less than 0.35 nm would be expected,[60] as found for the salt bridges between H13/H14 and E22/D23. This indicates that in the Aβ monomer there are indeed electrostatic interactions between E22/D23 and K28, but salt bridges are not formed. These are consistent with the recent experiment.[61] Our simulations also indicate that at pH 2.0 protonated E22 and D23 do not have obvious electrostatic interactions with K28 because the contact distances are peaked beyond 1.0 nm.

To test if these electrostatic interactions are persistent forces, we also analyzed the high-temperature simulation results (Table 2). It is surprising that even in such a large conformation pool (1 million candidates form 2 μs simulations) and at such high temperature (400 K) E22 interacts with H14 and H13 for 58% and 32% of the time, respectively, while D23 interacts with H13 and H14 for 43% and 36% of the time, respectively. Therefore, it is such persistent and specific interactions (E22 favors H14; D23 favors H13) that confine the conformational space of Aβ(10−35), which is less flexible at pH 5.6 than at low pH according to the number of clusters sampled (Table 1).

The low-pH simulation was used to mimic the double mutations of E22Q and D23N. Besides E22 and D23, E11 was also neutralized under the low-pH condition. To inspect whether this difference caused a problem, several short simulations for low pH (2.0) and the double mutations of E22Q and D23N were carried out, respectively. As shown in Table S2, the conformational propensities of the cc and strand-loop-strand structures derived from the two types of simulations were found to be similar. Analysis indicates that E11, which is at the N-terminal, is not involved in long-range contact with the central region and the C-terminal (17−35), which is essential to the formation of a special conformation (Figure 2). Experiments also showed that the N-terminal is highly flexible,[30] and no NOE data for the contact between E11 and the central region and the C-terminal (17−35) are available.[16] Therefore, the low-pH simulation should mimic the double mutation of the Aβ monomer reasonably well.

Simulations at High Temperature. One of the major limitations of our low-temperature simulations is that they do not approach equilibrium, as reflected in the growing number of clusters at the ends of the simulations (SI, Figure S5b). High-temperature simulations can greatly increase the speed of conformation sampling and system equilibrium. They have been successfully used in the characterization of denatured states, molten coils, and folding intermediates.[62−64] In addition, they also enable us to investigate the thermostability of the cc structure. We performed 20 simulations at 400 K (AβHT) starting from the cc structure. The combined simulation time was about 2 μs. The number of clusters reaches a plateau in these high-T simulations (SI, Figure S5a), indicating that the system nearly achieved conformational equilibrium.

The sampled conformations are highly heterogeneous. The number of clusters for AβHT is 2308 compared with 55 and 143 for AβHpH and AβLpH, respectively (Table 1). However, the average contact map of over one million conformations demonstrates that, even at such high temperature, some midrange and long-range contacts still exist (Figure 2e). Besides the strong interactions between charged groups (Table 2), these contacts include those between F19/F20 and the C-terminal as well as those between L34/M35 and the central hydrophobic core (L17-A21), with a contact probability larger than 20%, while F19 and I32 even have a contact probability greater than 30%. This implies the importance of F19 in defining the conformational features of the peptide, in agreement with the fact that the single-point mutation of F19T totally disrupts the ordered conformation.[21] The midrange contacts reveal the moderate persistence of the local loops spanning I31−L34, N27−I31, and, more profoundly, D23−K28.

Compared with the contact maps of AβHpH, it shows that a higher temperature diminishes the loop involved with F19−S26 centered at E22−V24 (Figure 1b) and intensifies the loop spanning D23−K28 centered at V24−S26. High temperature can denature peptides. Under such a condition, the secondary structures of peptides are biased in a way that reflects the intrinsic propensities of the local sequence.[65] It should be noted that no strong electrostatic interaction between E22/D23 and K28 could form at high temperature (Table 2). Thus, the latter loop may be determined by the sequence of D23−K28 at such high temperature. This is supported by NMR results that Aβ-(1−40), a longer peptide, has only αN(i, i+3) NOE in D23−

(60) Marqusee, S.; Baldwin, R. L. *Proc. Natl. Acad. Sci.* **1987**, *84*, 8898.
(61) Lazo, N. D.; Grant, M. A.; Condron, M. C.; Rigby, A. C.; Teplow, D. B. *Protein Sci.* **2005**, *14*, 1581.
(62) Wong, K. B.; Clarke, J.; Bond, C. J.; Neira, J. L.; Freund, S. M. V.; Fersht, A. R.; Daggett, V. *J. Mol. Biol.* **2000**, *296*, 1257−1282.
(63) Kazmirski, S. L.; Daggett, V. *J. Mol. Biol.* **1998**, *277*, 487−506.
(64) Mayor, U.; Guydosh, N. R.; Johnson, C. M.; Grossmann, J. G.; Sato, S.; Jas, G. S.; Freund, S. M. V.; Alonso, D. O. V.; Daggett, V.; Fersht, A. R. *Nature* **2003**, *421*, 863−867.
(65) Dyson, H. J.; Wright, P. E. *Nat. Struct. Biol.* **1998**, *5*, 499−503.

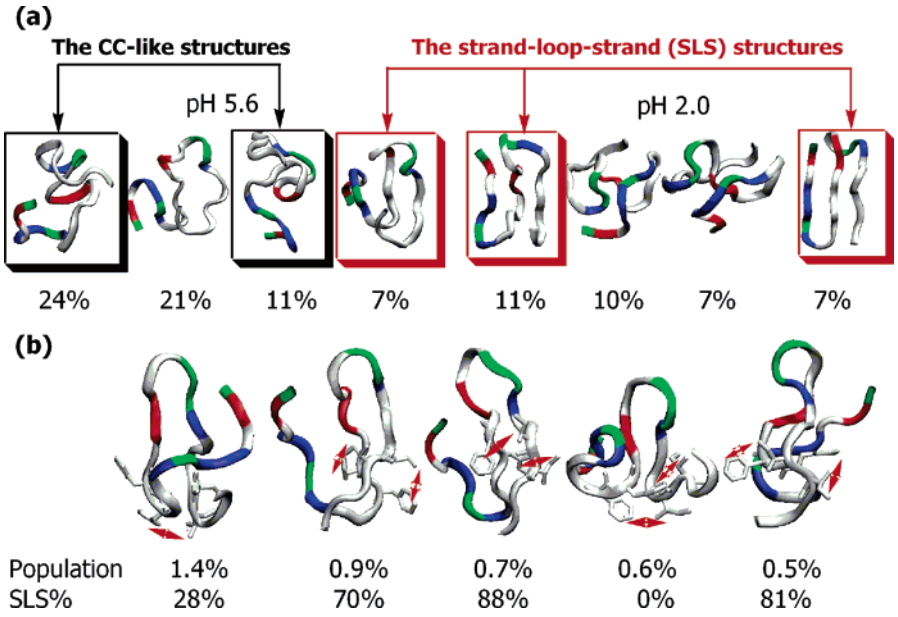

Figure 4. (a) The four most stable clusters of the AβHpH and AβLpH simulations and their populations (values below the structures). (b) The five most stable clusters of the AβHT simulation and their SLS probabilities. Red arrows indicate the hydrophobic interaction between F19/F20 and I31/I32.

S26 at pH 7.4, indicating a persistent loop, although the cc structure at pH 5.6 does not exist under this condition.[66]

Clustering Results. To explore more detailed conformational features, cluster analyses were performed for all the simulations according to the RMSD of all C_α's. The most populated clusters for each simulation are shown in Figure 4a,b. The two structures (black framed) are the major conformations in the first 0.6 μs of simulation at pH 5.6. They are similar in their N-terminus, close to that of the cc structure, but differ in the S26−M35 region. The third one resembles the cc structure more and is the representative conformation within the first 200 ns. However, the tertiary contact between ϵ-Me of M35 and the side chains of the central hydrophobic core is conserved for both conformations. The fourth populated cluster in the AβHpH simulation (red framed) occurs at around 0.8 μs. The topology of this cluster is different from that of the cc structure. It has a traversing loop spanning D23−K28 with two hydrophobic fragments, CHC and C-terminus, in antiparallel contact, forming a strand-loop-strand (SLS) structure (Figure 1c). It is intriguing that the first and fourth clusters (red framed) in AβLpH are also SLS-like, indicating that the SLS-like structures are the common conformational states accessible on the microsecond time scale for both pH values.

The five most stable clusters derived from the high-temperature simulations are also shown to be SLS-like. All of them have the persistent loop at D23−K28 and at least one hydrophobic contact between F19/F20 and I31/I32 (red arrows). Four of them have the CHC and C-terminus in antiparallel contact. These results imply that the SLS structure may be a special topology for Aβ(10−35).

The Strand-Loop-Strand Structure. The clustering results inspired us to try to filter all the conformations with the SLS topology from all the simulations. The conformational analysis tells us that this topology is hairpin-like in nature with the D23−K28 loop centered at V24−S26 and two antiparallel strands (Figure 1c). Thus, we used a set of intramolecular constraints between those close C_α's as filtration criteria, which can maintain the main features of the SLS topology (SI, Figure S6).

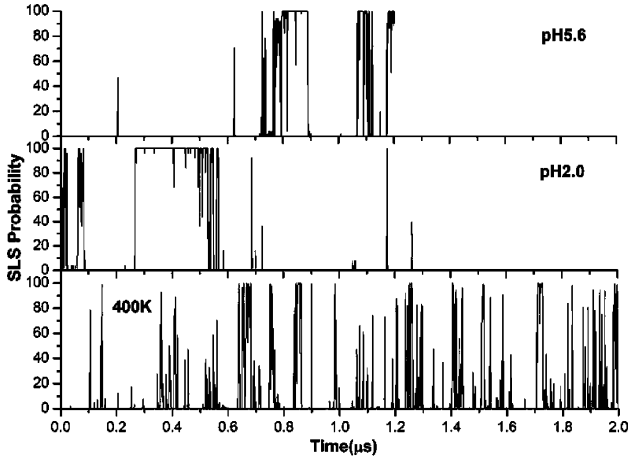

Figure 5. SLS probabilities for the three simulations. They are averages of every 100 frames.

Our results reveal that the SLS structures, at least topologically, are widely distributed at pH 5.6, pH 2.0, and high temperature (Figure 5). At pH 5.6, these structures appear mainly after 0.6 μs, while they can appear repeatedly at high temperature. The occurrence probabilities of the SLS structures are 14%, 21%, and 10% for AβHpH, AβLpH, and AβHT simulations, respectively. As expected, the average contact map over all SLS structures at 400 K shows the typical pattern with a hairpin-like conformation spanning K16−M35 (Figures 1c, 2f). The side chain contacts with probability larger than 50% include V18−L34, F9−I31/I32/G33, F20−I31, A21−A30/I31, E22−H14, and D23−N27/K28, as shown in Figure 6. Because the electrostatic interactions between E22/D23 and K28 are weak at this temperature (Figure S4b), the strong contacts between them may be hydrophobic since K28 also contains a long hydrophobic chain. The hydrogen bond (HB) map of the SLS structures (SI, Figure S2k) shows that no specific HB can have

(66) Hou, L.; Shao, H.; Zhang, Y.; Li, H.; Menon, N. K.; Neuhaus, E. B.; Brewer, J. M.; Byeon, I.-J. L.; Ray, D. G.; Vitek, M. P.; Iwashita, T.; Makula, R. A.; Przybyla, A. B.; Zagorski, M. G. *J. Am. Chem. Soc.* **2004**, *126*, 1992−2005.

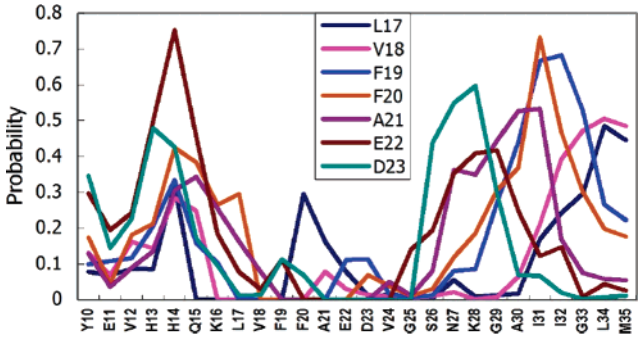

Figure 6. Contact probabilities of the side chains of L17-D23 with those of other residues.

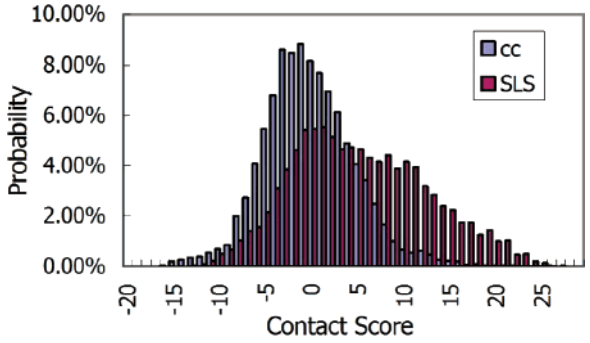

Figure 7. Probability distribution of the contact score C in AβHT with respect to the cc structure (blue) and the SLS structures (purple).

possibility exceeding 20% and the average number of HBs per SLS structure is about 3.6.

We also analyzed the stability of the cc and SLS structures by calculating the contact score C over all conformations sampled in the high-temperature simulations with respect to two models (the cc and SLS structures) based on their average contact maps (Figure 2b,f), respectively. The probability distributions of the C values with respect to the cc (cyan) and SLS (purple) structures are shown in Figure 7. In the AβHT simulations, only 0.70% of the conformations have C values greater than 15 with respect to the cc structure, while 11.76% of total population have C values larger than 15 with respect to the SLS structure. The maximum possible C values for the cc and SLS structures are 70 and 51, respectively, implying that this criterion does not overestimate the SLS structures. It can be concluded that the SLS structures do have superior thermostability to the cc structures at higher temperatures.

The SLS Topology Is Most Stable at 400 K. High-temperature simulations are close to equilibrium and sampled more heterogeneous conformations and enable us to evaluate the role of the SLS structure in the whole conformational pool. The clustering results have shown that there are 12 clusters with SLS probabilities larger than 50% within the 50 most stable clusters (accounting for about 20% of the total population). Thus the SLS topology comprises a series of stable conformations based on RMSD criteria.

To confirm that the SLS topology is the most stable at high temperature, we constructed a transition disconnectivity graph (TRDG), as shown in Figure 8. The vertical lines represent the 2308 conformation clusters. The partition function of each cluster (or the times the cluster is visited during simulations), Z_i (right axis), is represented by the bottom point (or node) of the line. The free energy of the cluster (left axis) can be calculated by $F_i = -kT \ln Z_i$.[51] Each vertical line (e.g., the line highlighted in red) connects with other vertical lines (e.g., the central line) at a branch point (the red spot). The height of this point denotes the transition probability from this cluster to the basin below the branch point (e.g., the basin containing all the clusters that connect with the central line at blue spots below the red spot). This probability is proportional to its partition function (Z_{ij}, right axis), the times of transition between the cluster and the basin. The larger the Z_{ij} is, the lower the barrier is.[51]

Overall, the FE surface is rugged. A large number of clusters are divided by relatively high barriers.[49] The stabilities of these clusters are close, due to the high temperature sampling. However, there is still an obvious basin composed of a bundle of stable clusters, centered with the second most stable cluster. It is considered as the representative node for this basin. Since this node is SLS-like, the SLS probability of the central basin was analyzed. Starting with the representative node, the total SLS population was calculated for the basin below a certain branch point at the central line when the height of this point (or barrier) gradually increases. The results are shown in Figure 8 (right). It reveals that the central region of the basin has high population of the SLS topology. Thus, the central basin consists of many stable SLS-like states that are separated by very low

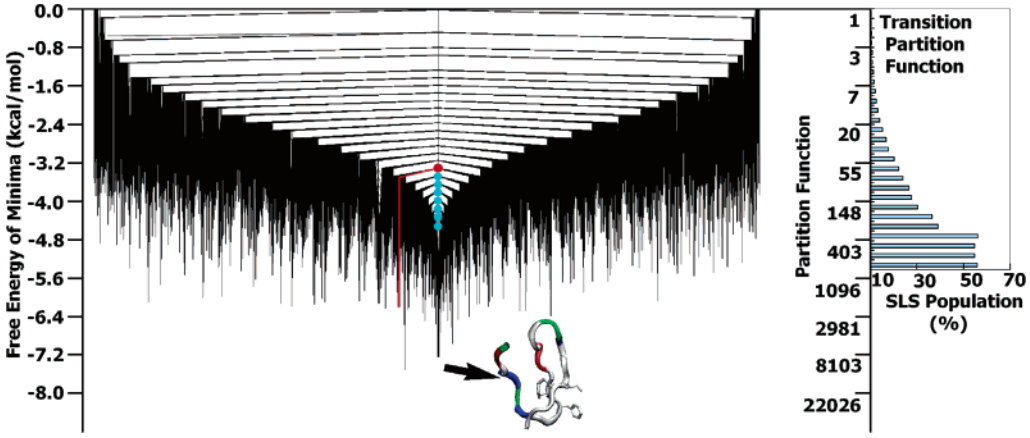

Figure 8. Transition disconnectivity graph of the AβHT simulations (left). Right vertical axis: partition function (Z_i) of clusters and transition ($Z_{i,j}$). Left vertical axis: free energy of the clusters. The right graph shows the SLS probability of the basin below a certain transition barrier (see text). It shares the partition function axis with the left graph.

FE barriers. If there is another stable topology other than the SLS, it should lead to another basin similar to the central one. Since such a basin is missing on the FE surface, we conclude that the SLS topology is most stable in our simulations at 400 K.

Summary. Our molecular dynamics simulations of Aβ(10−35) extend the time scale into microseconds. This allows us to make the following observations: (1) The collapsed-coil structure has a considerable stability under the experimental condition (pH 5.6), but can exchange with a strand-loop-strand (SLS) structure within microseconds. (2) When E22 and D23 are neutralized (pH 2.0), the SLS has a slightly enhanced stability, while the cc structure is essentially disrupted. (3) The SLS structure is the most stable topology at 400 K.

One concern with these simulations is the long-range electrostatic interactions since cutoff was employed for efficiency. An early study by Schreiber et al. emphasized the effect of cutoff on the stability of peptides.[67] Recently, Monticelli et al. showed that the long-range electrostatic interaction is important to stabilizing an antiparallel three-stranded β-sheet conformation.[58] To study the cutoff effect on our simulation results, we performed a series of short simulations (about 100 ns for each run) at 300 K and pH 5.6 with the particle-mesh Ewald (PME) method, starting with the SLS and cc structures, respectively. These simulations reveal that both the cc and SLS structures are stable, regardless of the force field used (Figure S7). Since the SLS structures are hairpin-like in nature, analogous to the results by Monticelli et al. for an antiparallel β-sheet, they are expected to be stabilized somewhat by the PME method. Furthermore, the numbers of NOE violations for the experimental models and for our simulation at pH 5.6 are quite similar, indicating that the simulation can reproduce most of the experimental observations. Therefore the appearance of the SLS structures and their stabilities may not be due to the cutoff effect.

The stability of the SLS structures is mainly due to an intrinsic propensity of the formation of the D23−K28 loop[61] and the hydrophobic contacts between the central hydrophobic core (L17−A21) and the C-terminal (A30−S35), possibly as well as interstrand HBs. It does not rely on the salt bridges between H13/H14 and E22/D23 (Table S2). On the other hand, the stability of the cc structures heavily relies on the salt bridge between H13/H14 and E22/D23. Thus, pH 5.6 is ideal for the formation of the cc structure, as found experimentally.[16] At pH 2.0 or at pH 7.5, no NMR signals for the cc structures could be found for the Aβ monomer.[16,66] In addition, these salt bridges are only necessary but not sufficient for the formation of the cc structures. For example, in our high-temperature simulations, these salt bridges are kept, but the cc structures are disrupted. This is due to the shift of the loop from F19−S26 (in the cc structure) to D23−K28 (in the SLS structure) when the temperature is raised. Inspection of the two families of experimental structures (Figure 1b) reveals that the stabilizing forces for the loop F19−S26 are all electrostatic, including hydrogen bonds of N27NH···F19CO, S26NH···A21CO, G25NH···A21CO, V24NH···Q22CO, and S26OH···A21CO. No hydrophobic contacts of side chains exist within the loop, and all the HBs are solvent-exposed. These imply that the loop F19−S26 should be vulnerable to solvent disturbance and thermal motion. On the other hand, besides the HBs, the loop D23−K28 is stabilized by the hydrophobic interactions between K28 and V24/D23 and contacts between D23 and S26/N27. According to a sequence structure analysis by Hutchinson and Thornton,[68] the fragments V24−G25−S26−N27 and G25−S26−N27−K28 are among those sequences most capable of forming reverse turns. This may explain why the loop D23−K28 is superior to the loop F19−S26 at high T and the SLS structures are thermally stable.

Both the experimental study by Esler et al. and the theoretical study by Massi et al. have systematically analyzed the kinetics of Aβ fibril elongation.[22,69] They proposed that the Aβ-soluble conformation (mainly the cc) can quickly dock onto fibril ends or undock, followed by a slow conformational rearrangement from Aβ (soluble) to Aβ (amyloid). According to our observation of multiple conformational exchanges of the Aβ monomer, it is likely that a large number of conformations can undergo such a two-step pathway. For each of them, its elongation rate is determined by two factors: (i) effective concentration of the conformation; (ii) the barrier height of the conformational rearrangement after the docking, because this is the rate-determining step. Therefore, a fast fibril elongation may require that the conformation has certain stability or population and its topology resembles the monomer structure in fibrils, so less conformational rearrangement is required.[70]

Therefore, we propose that the SLS structures are possible intermediates for fibril growth, because their topology resembles that in fibrils (Figure 1a,c) and they have considerable effective concentration, regardless of pH condition, temperature, and mutation. They should be available for binding at various conditions reported previously. Consequently, among all the parallel elongation pathways of different conformations, those of the SLS conformations may be more dominant for the overall rate.

Finally, Aβ(10−35) is aggregation-inactive at pH 2.0 in experiments, which has been attributed to the loss of the cc structures.[15] However, it cannot be excluded that the net charge of the peptide also influences aggregation.[71−73] The net charge is +2 at pH 5.6, but it becomes +5 at pH 2.0. The intermolecular repulsion due to the increased net charge may prevent aggregation. Such an explanation would not contradict our observation that the SLS structures are stable at low pH, and it could still be a binding intermediate. Recently, Fandrich et al. reported that at pH 1−3 the seeded aggregation of Aβ(1−40) readily occurs.[74] Another experiment also showed that at pH 1.0 Aβ can rapidly form a long filament, although the amount of fibrils is still small, possibly due to the rare presence of seeds.[75] This indicates that the Aβ monomer at low pH may still be able to elongate fibrils in the presence of seeds.

Acknowledgment. Dedicated to Professor Paul v. R. Schleyer on the occasion of his 75th birthday. This work was supported

(67) Schreiber, H.; Steinhauser, O. *Biochemistry* **1992**, *31*, 5857.
(68) Hutchinson, E. G.; Thornton, J. M. *Protein Sci.* **1994**, *3*, 2207.
(69) Massi, F.; Straub, J. E. *Proteins* **2001**, *42*, 217.
(70) Hall, D.; Hirota, N.; Dobson, C. M. *J. Mol. Biol.* **2005**, *195*, 195.
(71) Chiti, F.; Stefani, M.; Taddei, N.; Ramponi, G.; Dobson, C. M. *Nature* **2003**, *424*, 805.
(72) Schmittschmitt, J. P.; Scholtz, J. M. *Protein Sci.* **2003**, *12*, 2374.
(73) Fernandez-Escamilla, A.-M.; Rousseau, F.; Schymkowitz, J.; Serrano, L. *Nat. Biotech.* **2004**, *22*, 1302.
(74) Hortschansky, P.; Schroeckh, V.; Christopeit, T.; Zandomeneghi, G.; Fandrich, M. *Protein Sci*. **2005**, *14*, 1753.
(75) Harper, J. D.; Wong, S. S.; Lieber, C. M.; Lansbury, P. T., Jr. *Biochemistry* **1999**, *38*, 8972.

by the Research Grants Council of Hong Kong (HKUST6083/02M) and the National Natural Science Foundation of China (20225312). **Note Added in Proof.** Right after the submission of this paper, a study by Sciarretta et al. reported that a lactam bridge between D23 and K28 can greatly increase the rate of amyloid formation of Aβ (about 1000-fold) by helping D23−K28 to form a loop.[76] Another very interesting experiment by Lazo et al. reported that in Aβ a 10-residue protease-resistant segment, A21−A30, can adopt a loop conformation by NMR, with G25−S26 as a turn.[61] All these support our proposal of the existence of the SLS structure and its possible role in amyloid formation.

Supporting Information Available: Detailed information about the setup for various MD simulations (Tables S1, S2), clustering method, transition disconnectivity graph, and criteria for filtering the SLS structure, Figures S1−S7, are available free of charge via the Internet at http://pubs.acs.org.

JA051699H

(76) Sciarretta, K. L.; Gordon, D. J.; Petkova, A. T.; Tycko, R.; Meredith, S. C. *Biochemistry* **2005**, *44*, 6003.